Journal of Power Sources 192 (2009) 494–501

Contents lists available at ScienceDirect

Journal of Power Sources

journal homepage: www.elsevier.com/locate/jpowsour

Optimized temperature control system integrated into a micro direct methanol fuel cell for extreme environments

Qian Zhang[a], Xiaohong Wang[a,*], Yiming Zhu[a], Yan'an Zhou[a], Xinping Qiu[b], Litian Liu[a]

[a] Institute of Microelectronics, Tsinghua University, Beijing 100084, PR China
[b] Department of Chemistry, Tsinghua University, Beijing 100084, PR China

ARTICLE INFO

Article history:
Received 21 January 2009
Received in revised form 4 March 2009
Accepted 4 March 2009
Available online 19 March 2009

Keywords:
Micro fuel cells
DMFC
Temperature control
Temperature distribution
Heater
Temperature sensor

ABSTRACT

This paper reports a micro direct methanol fuel cell (μDMFC) integrated with a heater and a temperature sensor to realize temperature control. A thermal model for the μDMFC is set up based on heat transfer and emission mechanisms. Several patterns of the heater are designed and simulated to produce a more uniform temperature profile. The μDMFC with optimized temperature control system, which has better temperature distribution, is fabricated by using MEMS technologies, assembled with polydimethylsiloxane (PDMS) material and polymethylmethacrylate (PMMA) holders, and characterized in two methods, one with different currents applied and another with different methanol velocities. A μDMFC integrated with the heater of different pattern and another one with aluminum holders, are assembled and tested also to verify the heating effect and temperature maintaining of packaging material. This work would make it possible for a μDMFC to enhance the performance by adjusting to an optimal temperature and employ in extreme environments, such as severe winter, polar region, outer space, desert and deep sea area.

1. Introduction

With the increasing functionalities of portable devices, the demand for more reliable, longer lasting and clean power sources has been rising rapidly. A micro direct methanol fuel cell (μDMFC) is a very promising power source for military equipments, portable devices and microsystems due to its high energy density, easy recharging, low pollution, low temperature operation, etc. [1–4]. However, there are several technological challenges that have to be worked out before the μDMFC can be truly attractive for commercialization, such as relatively low power density, management of heat and water, slow reaction kinetics of methanol electrooxidation, methanol crossover, fuel transport, etc. Most of the previous researches have been focusing on these challenges and achieved certain results [5–11].

Temperature influence on the performance is still a fundamental problem for the development of μDMFC systems. A μDMFC has not optimal performance at lower temperature, even does not work below the freezing point of methanol solution, although it has a significant advantage of which it can work at room temperature. Characteristics of polymer electrolyte membrane fuel cell (PEMFC) were examined with thermal cycles during which the temperature of the environment was cycled from 80 to −10 °C by Cho et al. [12]. The cell performance was degraded by deteriorating the structure of the membrane electrode assemblies (MEAs) due to the phase transformation and volume changes of water. This is particularly problematic in application for portable devices because such devices may be used in cold environments, such as severe winter, polar region, outer space, desert and deep sea area. In addition, the proton exchange membrane (PEM) is only stable for a narrow temperature range because its conductivity is affected by humidification. Too high temperature may lead to PEM dry-out or even the sulfonate group decomposition [13]. Therefore it is necessary for a μDMFC to maintain an appropriate operating temperature, especially in extreme environments.

Temperature is an important factor affecting the performance of a μDMFC. Although a number of papers on thermal management have been published, most of them focus on modeling and simulation [10,14]. A thin film temperature sensor was developed for application in an operating PEMFC by He et al. [15]. They used a structured gold film as a temperature sensor on the Nafion membrane to monitor the operating temperature. Lee et al. presented a micro thermal sensor integrated into a micro fuel cell. The Platinum (Pt) metal is deposited as a micro thermal sensor on the rib [16]. A separate testing system was established for the purpose of testing the performance of μDMFC in the wide range of temperature by Li et al. The brass heating block was fabricated to heat up the methanol solution [17]. It is indicated that the temperature

* Corresponding author. Tel.: +86 10 62789151x317; fax: +86 10 62771130.
E-mail address: wxh-ime@tsinghua.edu.cn (X. Wang).

0378-7753/$ – see front matter © 2009 Elsevier B.V. All rights reserved.
doi:10.1016/j.jpowsour.2009.03.013

control is necessary for the operating and testing of a μDMFC. A temperature control system which consists of a heater and a temperature sensor, is needed actually for a μDMFC to stably operate, especially when it is placed in extreme climates or unconditioned environments. However, none of the reported works implemented the temperature control system integrated into the fuel cells.

This paper presents a μDMFC integrated with a heater and a temperature sensor to realize temperature control [18]. For improving the heating effect, the pattern of heater is optimally designed, based on the thermal analysis. Micromachining technologies are developed to realize the optimized design by fabricating the plates integrated with temperature control devices. Two μDMFCs with different patterns of heater are assembled with polydimethylsiloxane (PDMS) materials and polymethylmethacrylate (PMMA) holders, and characterized to compare their heating effect. Another μDMFC assembled with aluminum holders also is measured to verify the temperature maintaining of packaging material. The μDMFC with temperature control system would show great potential application to enhance the performance by adjusting to an optimal temperature and employ in extreme environments.

2. Design and simulation

As an electrochemical device, the μDMFC converts the chemical energy to electrical energy directly. The schematic of the μDMFC, which consists of the MEA sandwiched between two silicon plates, is shown in Fig. 1. During the operation, an aqueous methanol solution is fed to anode and oxidized to carbon dioxide, protons, and electrons at anodic catalyst layer. The protons migrate directly through the PEM to the cathode. The electrons flow through an external circuit to the cathode where they combine with oxygen and protons to produce water, forming an electrical current as a result.

2.1. Temperature influence

The performance of a μDMFC is influenced significantly by the temperature, although it has that advantage that it can work at room temperature, it does not work when liquid freezes at temperature below the freezing point of methanol solution especially. And the cell performance is improved with an increase of the temperature in a certain range because the conductivity of the PEM and the reaction kinetics at both anode and cathode are enhanced. The temperature influence on the μDMFC can be investigated by a mathematical model. The work about the electrochemical equations and parameters can refer our previous publication [19].

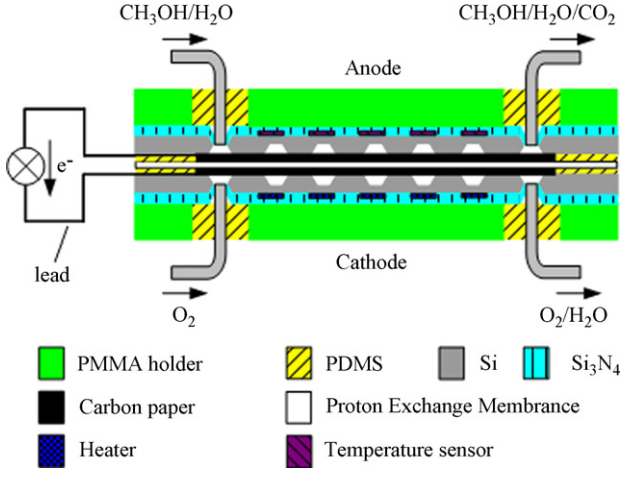

Fig. 1. Schematic of the μDMFC integrated with a heater and a temperature sensor.

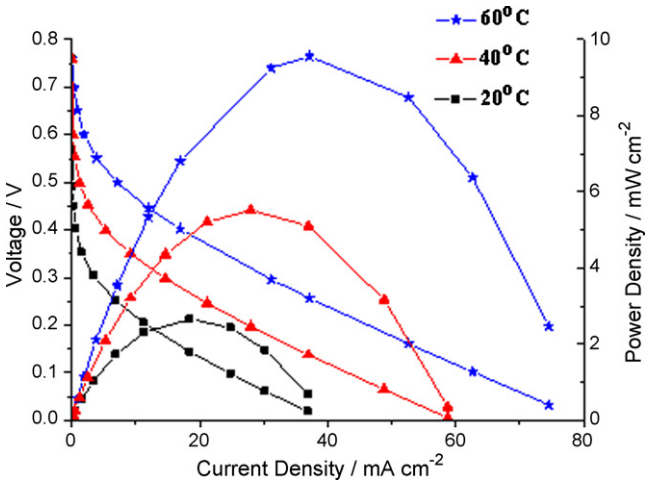

Fig. 2. The simulation results of the temperature influence on the μDMFC performance.

Fig. 2 presents the simulation results of the temperature influence on the μDMFC performance. It can be seen obviously that the temperature affects the performance much significantly. The μDMFC at 60 °C shows 3.6 times larger power density than that at room temperature. It is demonstrated theoretically that the cell performance can be improved with an increase of the temperature in a certain range due to the fast reaction kinetics. Therefore temperature increasing and maintaining are important for performance improvement and application in extreme environments.

2.2. Structure design

The temperature control system integrated into a μDMFC consists of a heater and a temperature sensor, as shown in Fig. 1. The heat is generated from the heater applied by a current, and emitted in several ways for a μDMFC including heat taken away by the methanol solution, thermal convection, radiation, etc. So, a heater is designed on the cathode plate to increase temperature. And a temperature sensor is integrated into the anode plate to measure the steady operating temperature.

The heat transfer in a μDMFC is analyzed in order to design the structure of the plate integrated with temperature control device. Considering the transfer of heat across a membrane, the heat, Q, is related to the temperature gradient as

$$Q = k_m A_m \frac{T_1 - T_2}{L_m} \quad (1)$$

where k_m is the thermal conductivity coefficient of the membrane, A_m is the surface area of the membrane, L_m is the thickness of the membrane, and $T_1 - T_2$ is the temperature difference on two sides of the membrane. A thermal oxide is used to insulate the temperature control device from the silicon wafer as dielectric layer. For the fuel cell, the heat transfers across the plate consisting of the silicon wafer and dielectric layer. The temperature difference on two sides of silicon wafer and dielectric lay can be neglected due to the higher thermal conductivity of the silicon and the thinness of the thermal oxide. Therefore, the flow field channel and the temperature control device are designed on the two sides of the plate respectively, as shown in Fig. 3. It is a great improvement for fuel cell performance that the temperature control device, not placed on the rib, would not reduce the area of current collecting layer. Pt resistance, with a linear temperature response in a wide temperature range, remains stable and does not undergo any significant physical or chemical changes. Pt is therefore a very suitable material as the temperature sensor.

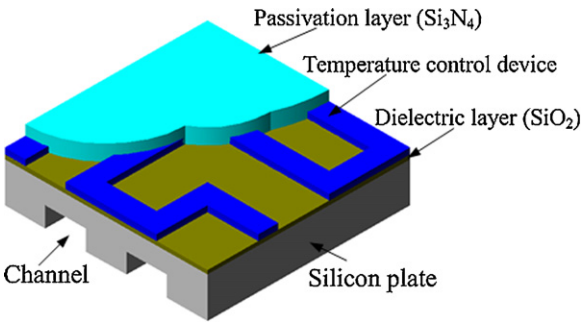

Fig. 3. Cross-section schematic of the silicon plate with the temperature control device.

2.3. Thermal model

A thermal model is set up to estimate thermal behavior of the μDMFC. The heat generation by electrochemical reactions occurring in the catalyst layers and by the heater is considered. The thermal loss that makes a great negative impact on maintaining an optimal temperature is also studied. The heat taken away by the methanol solution, thermal convection, radiation, and heat emission through the lead are considered as main thermal loss ways.

According to the Reynolds number, the methanol solution flow in the channels is laminar flow. The heat loss amount by the methanol solution (Q_{meth}) is calculated by

$$Q_{meth} = \rho v C_P (T - T_0) \quad (2)$$

where T is the operating temperature, T_0 is the environment temperature, and v, C_P, and ρ are flow velocity, heat capacity, and density of the methanol solution, respectively. For an active μDMFC, the methanol solution, like cooling liquid, carries out a lot of heat. It can be seen obviously from the formula that the heat taken away by the methanol solution is proportional to the flow velocity.

The heat loss amount by thermal convection and radiation ($Q_{con,rad}$) is given by

$$Q_{con,rad} = hA(T_W - T_0) + \varepsilon\sigma A(T_W^4 - T_0^4) \quad (3)$$

where h is convective heat transfer coefficient, A is the surface area, T_W is the surface temperature of a μDMFC, ε is emissivity, and δ is Stefan-Boltzmann constant. The lower surface temperature contributes to reduce the thermal convection and radiation. The heat transfers to the surface of a μDMFC through the packaging material. Based on the formula (1), the surface temperature is determined by the thermal conductivity coefficient of the packaging material. The material with low thermal conductivity coefficient has better effect of temperature maintaining.

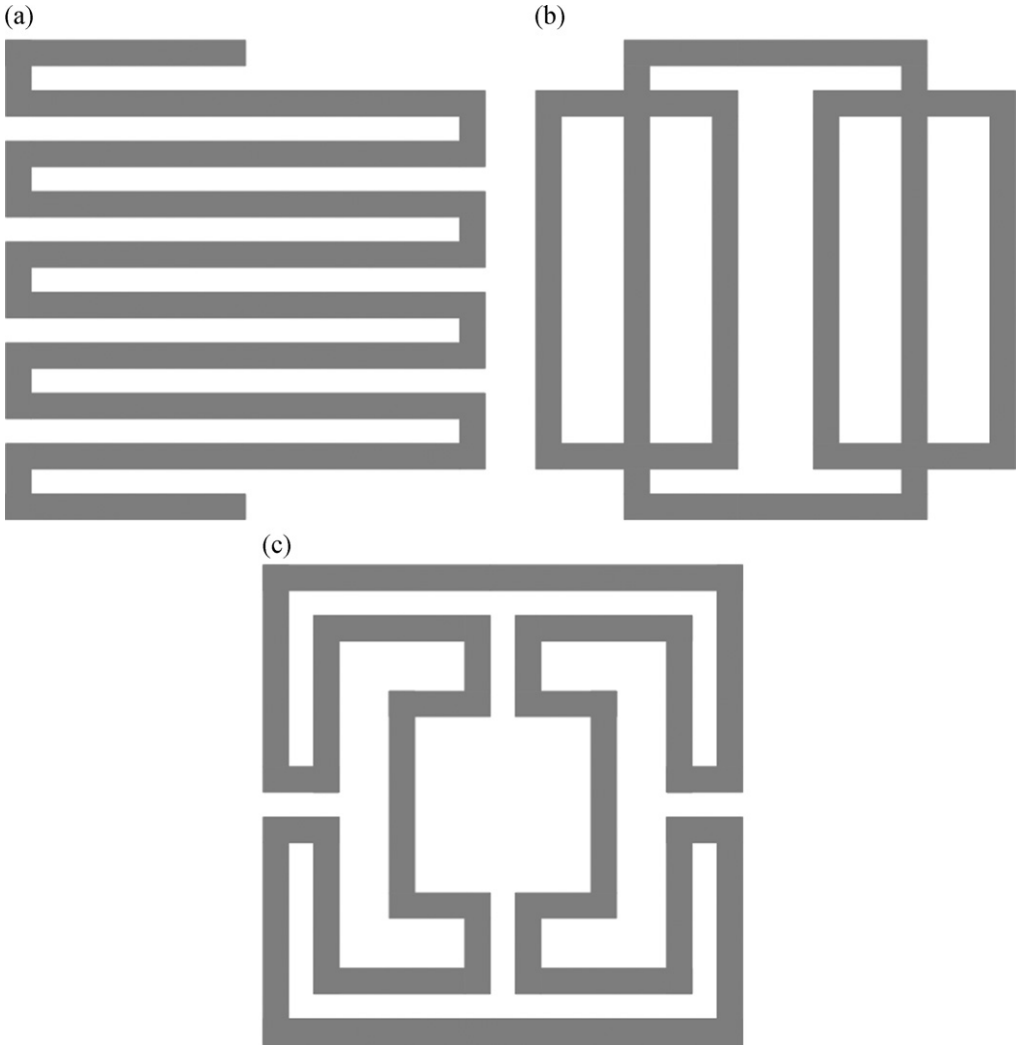

Fig. 4. Patterns of the heater: (a) serpentine pattern, (b) strip pattern, and (c) square pattern.

The heat loss amount through the lead (Q_{lead}) is expressed by

$$Q_{lead} = \sqrt{hPk_lA_S}(T - T_0) \quad (4)$$

where P, A_S, and k_l are cross-section perimeter, cross-section area, and thermal conductivity coefficient of the lead, respectively, which are determined by the material and structure of the lead. The heat loss amount through the lead is much less than that by the methanol solution and thermal convection and radiation.

It is necessary to invoke some assumptions to make the complex system simpler. The fuel cell is assumed to operate under steady-state conditions. Temperature gradients inside the cell, especially between the anode and cathode, are negligible. Joule heat caused by the current flow through each component is ignored. Heat exchange with the oxygen in the cathode channel is negligible. The heat capacity of the methanol solution is much larger than that of the oxygen and thus the contribution of gas cooling to the overall heat balance is small.

2.4. Simulation and optimization

Several patterns of heater are designed to investigate their influence on the thermal distributions and optimize the heating effect. The heater pattern has a great influence on the heating effect because the temperature distribution is determined by the position of the heat source on a plate. The heater structure, which tends to suffer from an uneven thermal distribution, could lead to an uneven catalytic reaction and hence reduce the performance of the μDMFC. Three patterns are shown in Fig. 4 that we refer to as (a) serpentine pattern, (b) strip pattern, and (c) square pattern.

Full simulations have been carried out in order to investigate the performance of the heater designs. A set of three-dimensional simulations was conducted using ANSYS that employs Finite Element Analysis (FEA). Different patterns of the heater are simulated and compared to optimize the heating effect. The thermal–electric coupled analysis mode is applied on the simulation during the FEA procedure. The heat flux is set to flow from the constant heat source to the plate while heat is dissipated into the air from both sides of the plate. Voltage and thermal convection loads are defined as boundary conditions. The resistance of each heater can be measured by simulation so a proper voltage can be set corresponding to the resistance. The values of voltage loads are fixed according to the different values of resistance so that every heater generates the same heat amount. The thermal convection loads are applied on the surface of the model to indicate the heat dissipation through convection and radiation between the fuel cell and external environment. The heat taken away by the methanol solution is equivalent to thermal convection as well, only with different coefficient of thermal convection. Considering the methanol flow velocity of 0.4 mL min^{-1}, the temperature distributions of different patterns of the heater are shown in Fig. 5.

The simulation results show that the heaters applied by a current generate heat to increase the operating temperature with different

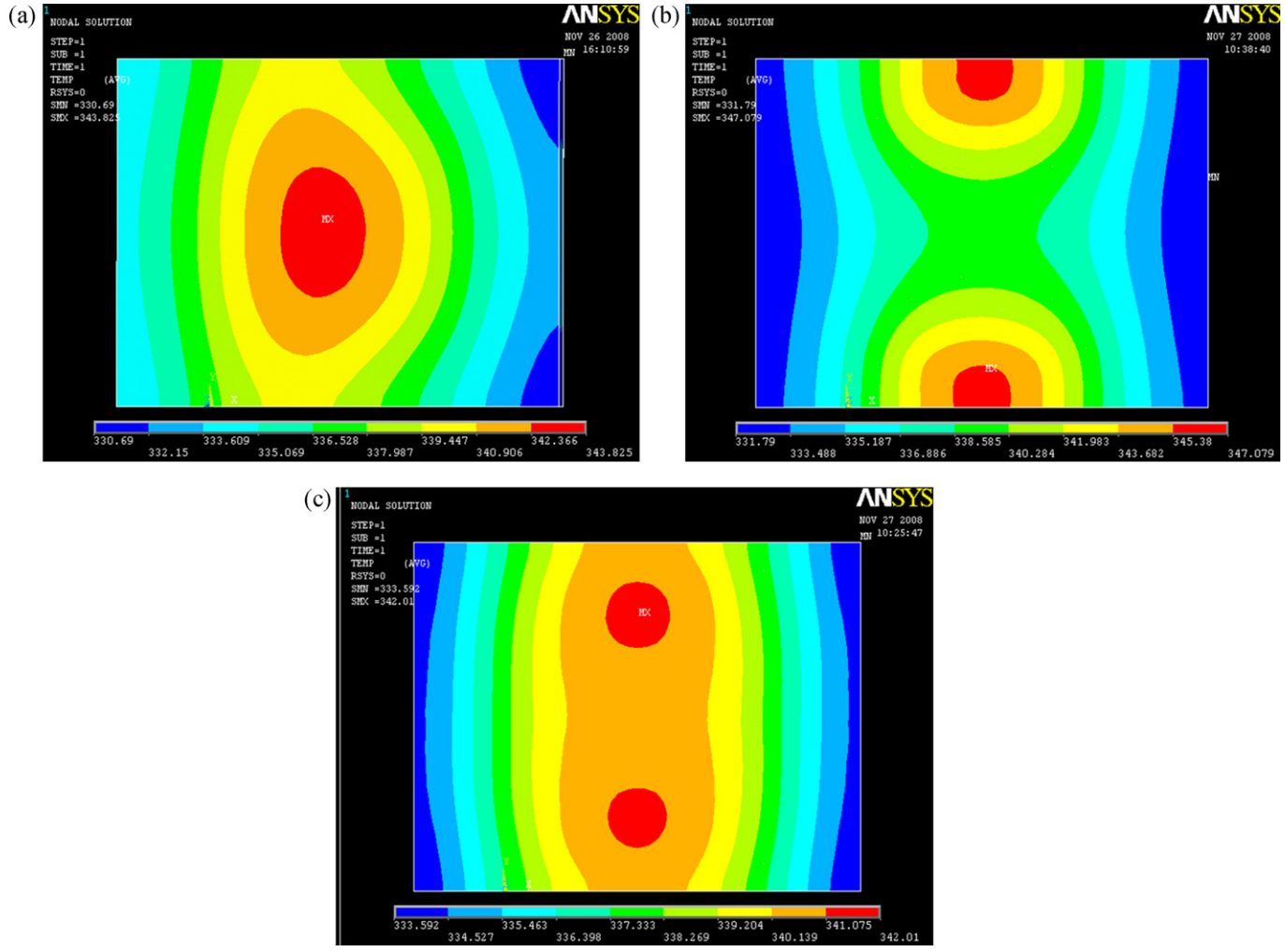

Fig. 5. Simulation results: (a) temperature distribution caused by heater of serpentine pattern, (b) temperature distribution caused by heater of strip pattern, and (c) temperature distribution caused by heater of square pattern.

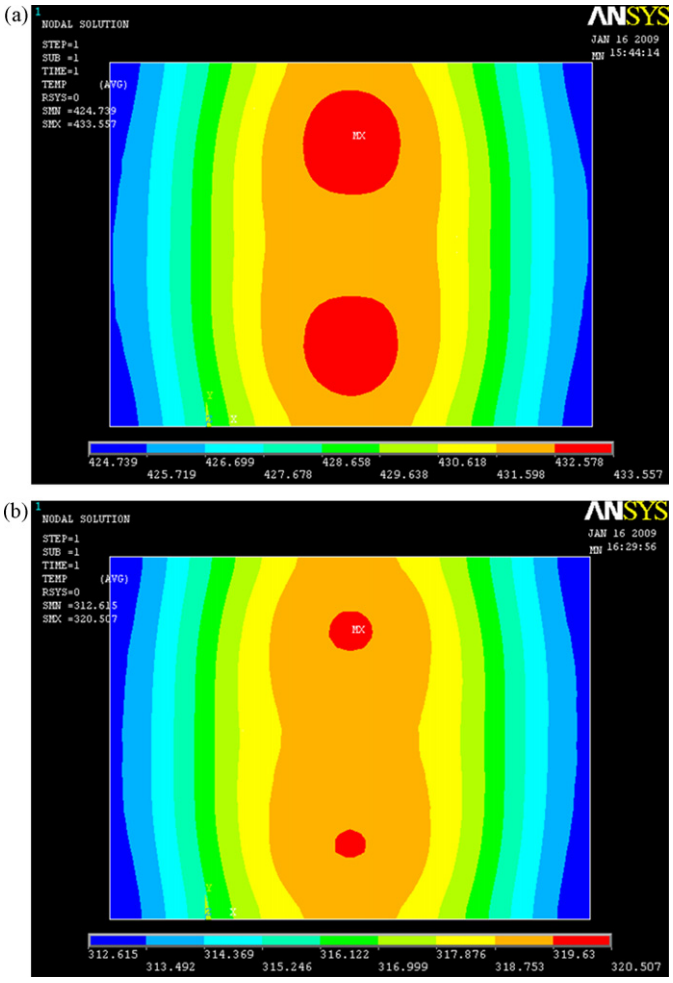

Fig. 6. Simulation results of different flow velocities for the square pattern: (a) temperature distribution with the flow velocity of 0.1 mL min^{-1}, and (b) temperature distribution with the flow velocity of 0.8 mL min^{-1}.

temperature distributions on the plate of a fuel cell. The heater of serpentine pattern produces a central hot spot as shown in Fig. 5(a). The temperature falls around and makes a maximum difference of 13 °C. The heater of strip pattern causes hot spots at the main circuits of six branches because the bigger current passes through the main circuits, as shown in Fig. 5(b), with a 15 °C of the maximum difference in temperature. The heater of square pattern which has two branch circuits and leaves space in the center, provides the most even temperature distribution and maximum difference in temperature of 8 °C, as shown in Fig. 5(c).

The heater of square pattern on the plate with different methanol flow velocities is simulated to quantify the thermal loss by flowing methanol solution. The heater produces the same temperature distributions on the plate because different methanol flow velocities present different coefficient of thermal convection. The simulation result in Fig. 6 shows the temperature distribution profile with methanol flow velocities of 0.1 and 0.8 mL min^{-1}. The heater causes the operating temperature of 157, 65, and 44 °C with the flow velocities of 0.1, 0.4, 0.8 mL min^{-1}, respectively. It is obvious that the increasing flow velocity results in decreasing operating temperature due to more heat taken away by the methanol solution.

3. Fabrication and assembly

The fabrication process of the anode and cathode plates is presented in Fig. 7 and described in detail as follows. (a) Thermal oxide and LPCVD Si_3N_4 are deposited on both sides of a 400 μm thick 3 in. double-polished ⟨1 0 0⟩ silicon wafer. (b) Double-side lithography technology is introduced to form complicated flow patterns of the anode and cathode plates. (c) KOH-timed etching is employed to anisotropically etch the silicon wafer until the flow patterns and the feeding hole are formed. (d) A thermal oxide of 0.1 μm is grown as the dielectric membrane. (e) The patterns of the heater and the temperature sensor are formed by lithography technology. (f) Pt with an adhesive layer of Ti (0.2 μm thick) is sputtered to pattern using a lift-off process for making the heater and the temperature sensor on the back. (g) The temperature control devices are covered with a 0.3 μm PECVD Si_3N_4 as the passivation layer. (h) Ti/Pt is sputtered to form the current collecting layer on the front.

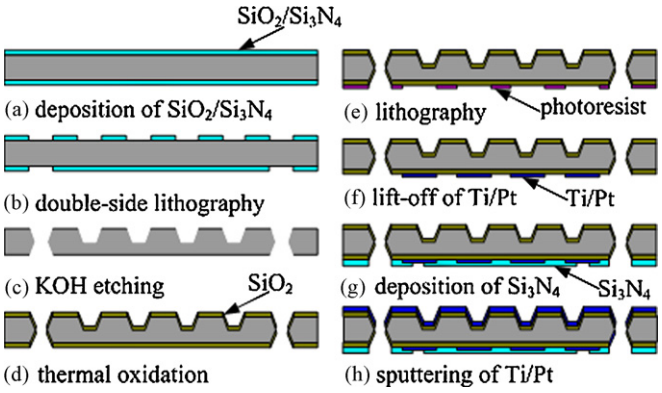

Fig. 7. Microfabrication process of the μDMFC anode and cathode plates.

The anode and cathode plates are fabricated simultaneously on the same wafer with identical process. Double-side lithography halves KOH etching time as mentioned in our previous work [20]. Fig. 8 shows the two sides of the cathode plate fabricated, the flow channel on the front and the heater on the back. The heater with square pattern is shown as Fig. 8(b). The heater is located on the active area of 6.8 mm × 6.8 mm to enhance the heating efficiency.

The MEA consists of two hot pressing wet-proof catalyst-coated (anode: 4.0 mg cm^{-2} Pt–Ru, cathode: 1.5 mg cm^{-2} Pt) carbon papers which are used as the diffusion layer, and a layer of Nafion117 in between.

PDMS and PMMA holders are used to keep the fuel cell from leakage and protect fragile silicon plates. The flexibility and chemical inertness of PDMS exactly satisfy the assembly requirements of the μDMFC. As previous work has mentioned, the prefabricated PDMS pieces have functions in the packaging: the sealing gaskets around both sides of MEA, the buffering layers between plates and corresponding holders, and the fixture of feeding tubes. The PMMA holders are employed to provide a uniform pressure over the whole plate area and improve the contact between components as the aluminum holders used in our previous work [20]. The μDMFC integrated with the heater of square pattern assembled by PMMA holders is shown in Fig. 9, and the detailed parameters are listed in Table 1.

Table 1
Parameters of the μDMFC integrated with a heater and a temperature sensor.

Total size, including holders	23 mm × 15 mm × 6.1 mm
Plate area	20 mm × 12.8 mm
Active area	6.8 mm × 6.8 mm
Channel/rib width	0.4 mm
Channel depth	0.2 mm
Heater resistance (25 °C)	239 Ω
Sensor resistance (25 °C)	169 Ω

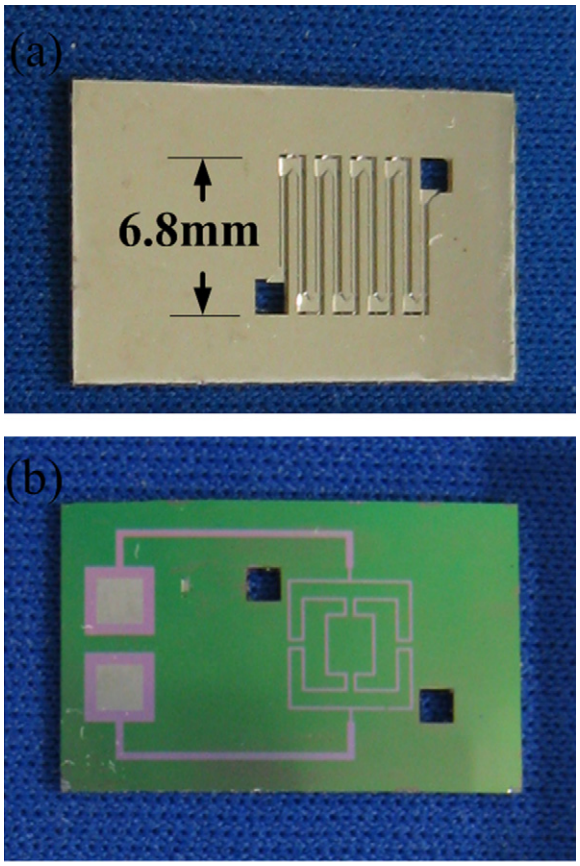

Fig. 8. Photos of the cathode plate: (a) the flow channel on the front of the cathode plate, and (b) the heater of square pattern on the back of the cathode plate.

4. Results and discussion

4.1. Calibration of the temperature sensor

Since the temperature sensor is not a standard component, a calibration is determined before the cell performance test. The plate with the temperature sensor is placed in an adjustable oven, and calibrated during the temperature changing process.

A plot calibrated of the temperature sensor resistance vs. temperature can be illustrated by using the method of fitting a straight line to data points. The temperature sensor resistance is calculated as

$$R = R_0[1 + \alpha(T - T_0)] \quad (5)$$

where R_0 is the sensor resistance at room temperature ($T_0 = 25\,^{\circ}C$), and α is the temperature coefficient of the resistance. The curve shows that the temperature sensor has a linear response of $\alpha = 0.0025\,^{\circ}C^{-1}$ in the range of 25–70 °C temperature. When the μDMFC operates at a certain temperature, the sensor resistance (R) is measured and the temperature is calculated as

$$T = T_0 + \frac{R - R_0}{\alpha R_0} \quad (6)$$

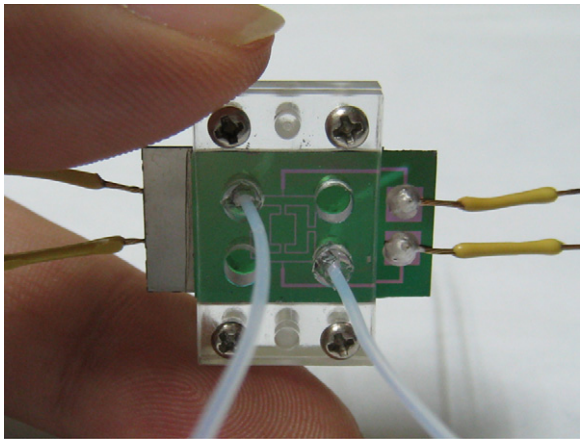

Fig. 9. The μDMFC integrated with the heater of square pattern assembled by PMMA holders.

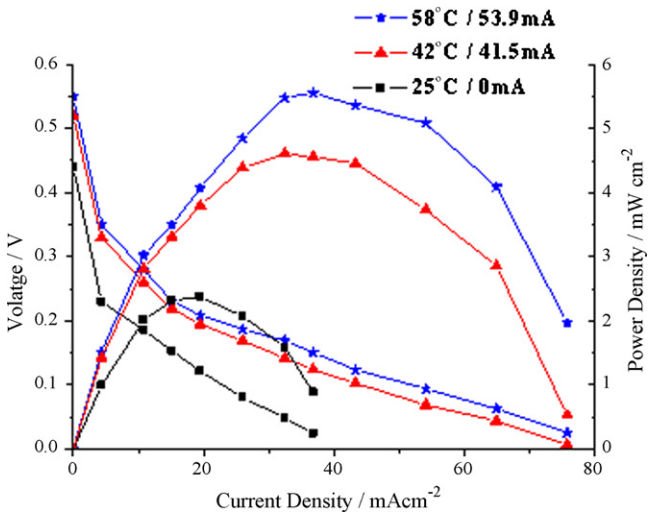

Fig. 10. Performance of the μDMFC integrated with the heater of square pattern assembled by PMMA holders, with 2 M methanol solution under 0.1 mL min^{-1} methanol flow rate, when different currents are applied to the heater.

4.2. Performance vs. temperature

The performance of the μDMFC integrated with the heater of square pattern assembled by PMMA holders is measured on an electrochemical interface, Solartron SI1287. The methanol solution is driven by a horizontal pump. A constant current is applied and the output voltage is monitored for a period (50 s in this paper) until the final steady-state value is recorded.

Fig. 10 depicts the performance of the μDMFC when the currents applied to the heater are 53.9, 41.5, and 0 mA, respectively. The corresponding operating temperatures measured by the sensor are 58, 42 °C and room temperature (25 °C). The experimental results show that the prototype has the maximum power density of 5.55 mW cm^{-2} at 58 °C, which is more twice higher than that of the μDMFC at the value of 2.37 mW cm^{-2} at room temperature, using 2 M methanol solution under 0.1 mL min^{-1} methanol flow rate. Obviously, the cell temperature is raised with the increasing current applied to the heater for more heat generated from the heater. Unfortunately, it is also found that the cell performance is lower than our previous work [21]. 2000 Å Ti/Pt layer, instead of 8000 Å Ti/Cu and 2000 Å Au, is used for current collection layer in this work. The resistance of the thinner current collection layer made by Ti/Pt (about 3 Ω) is larger than that by Ti/Cu/Au (about 0.5 Ω). This probably results in the larger internal resistance of the μDMFC (5–6 Ω) and the lower performance.

4.3. Performance vs. flow velocity

As mentioned above, the heat taken away by the methanol solution, accounting for a major proportion in the total thermal loss, is proportional to the flow velocity. The thermal loss is studied

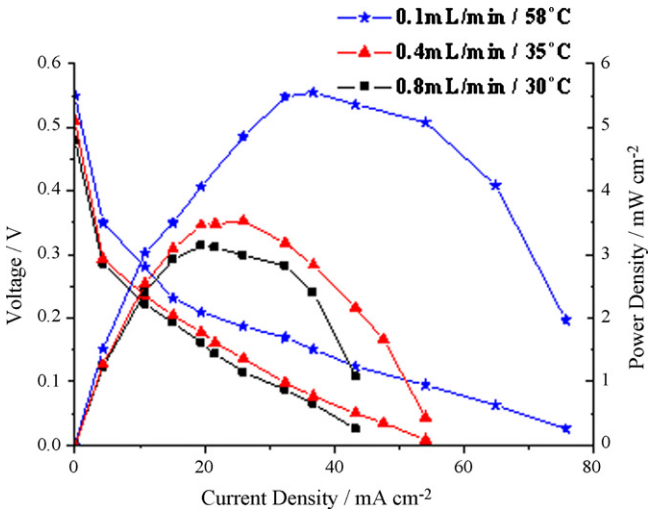

Fig. 11. Performance of the μDMFC integrated with the heater of square pattern assembled by PMMA holders, under different methanol velocities with 2 M methanol solution, when a current of 53.9 mA is applied to the heater.

experimentally to verify the great negative impact on maintaining an optimal temperature. Fig. 11 illustrates the performance of the μDMFC under the methanol solution flow velocities of 0.1, 0.4, 0.8 mL min^{-1} with 2 M methanol solution, when a current of 53.9 mA is applied to the heater. The corresponding operating temperatures measured by the sensor are 58, 35 and 30 °C. The maximum power density is 5.55 mW cm^{-2} under 0.1 mL min^{-1}, 3.52 mW cm^{-2} under 0.4 mL min^{-1}, and 3.13 mW cm^{-2} under 0.8 mL min^{-1}. The experimental results show that the performance is improved with a decrease of the flow velocity, which is matched with the previous simulations results, because the low velocity contributes to less thermal loss and high operating temperature in the μDMFC. For a μDMFC without temperature control system, the performance is improved with an increase of the methanol solution flow velocity as the high velocity contributes to an efficient removal of CO_2. Therefore, the flow velocity needs to balance the thermal loss and the removal of CO_2 when temperature control system is applied to the μDMFC.

4.4. Performance comparison of different patterns of heater

A μDMFC integrated with the heater of strip pattern assembled by PMMA holders, as shown in Fig. 12, is characterized also when the currents are applied. The heater of strip pattern applied by a current of 54.9 mA generates the same heat amount as that of square pattern applied by a current of 41.5 mA. The maximum power density is 3.15 mW cm^{-2} under the current of 54.9 mA applied, and 2.21 mW cm^{-2} under no current applied, as shown in Fig. 13. The μDMFC integrated with the heater of square pattern has better performance than that integrated with the heater of strip pattern, when the same heat amount is applied. Considering the different contact situations between MEA and plate, the maximum power density is inversely proportional to the internal resistance at Ohmic Region. The comparison results are listed in Table 2. It is indicated that the heater of square pattern enhances the performance than that of strip pattern because the even thermal distribution results in the even catalytic reaction, acting in accord with the simulation result.

4.5. Performance comparison of different packaging materials

A μDMFC integrated with the heater of square pattern assembled by aluminum holders is also measured to compare the temperature maintaining. The operating temperature of μDMFC

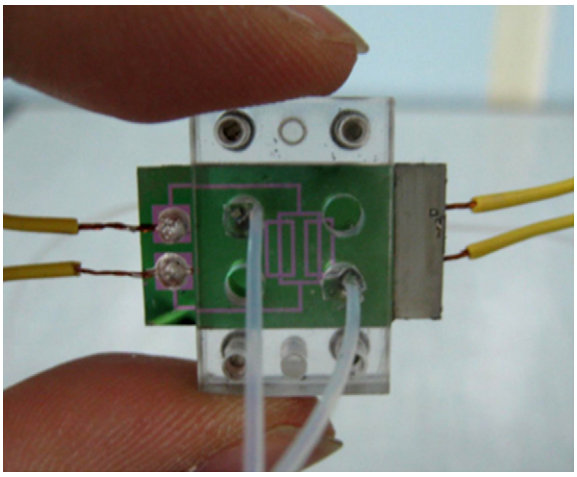

Fig. 12. The μDMFC integrated with the heater of strip pattern assembled by PMMA holders.

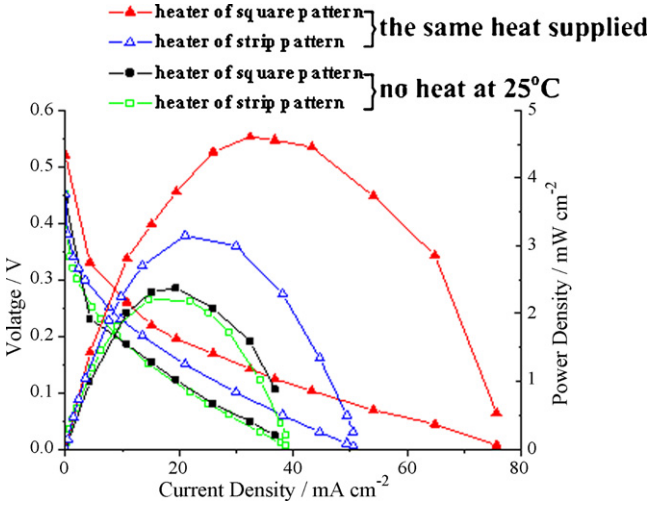

Fig. 13. Performance comparison of the μDMFCs integrated with the heater of different pattern assembled by PMMA holders with 2 M methanol solution under 0.1 mL min^{-1} methanol flow rate, when the same heat amount is applied.

assembled with PMMA and aluminum holders are 42 and 36 °C, respectively, when the same heat amount is applied as shown in Fig. 14. The maximum power densities measured of the two cells are 4.61 and 3.28 mW cm^{-2}, respectively, while corresponding internal resistances are 5 and 6.2 Ω, as listed in Table 2. Considering the influence of internal resistance on the cell performance as mentioned above, the maximum power densities normalized are 4.61 and 4.07 mW cm^{-2}, respectively. According to the comparison

Table 2
Performance and internal resistance of the three μDMFCs.

	Internal resistance (Ω)	Maximum power density (mW cm^{-2})	Operating temperature (°C)
μDMFC 1, heater of square pattern and PMMA holders	5	4.61	42
μDMFC 2, heater of strip pattern and PMMA holders	5.7 (5)	3.15 (3.59)	33
μDMFC 3, heater of square pattern and aluminum holders	6.2 (5)	3.28 (4.07)	36

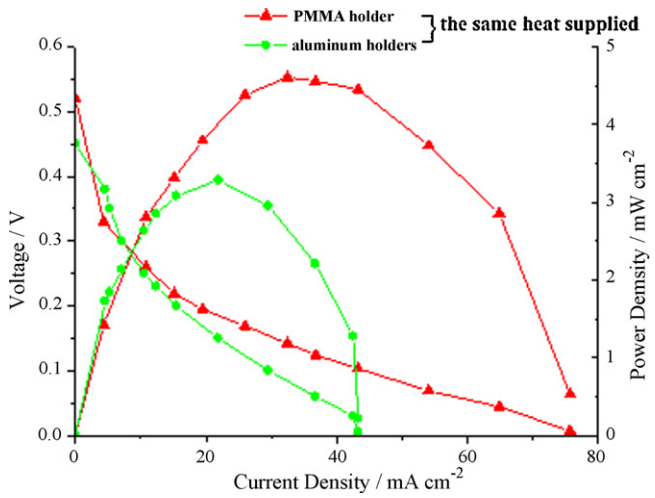

Fig. 14. Performance comparison of the μDMFCs integrated with the heater of square pattern assembled by different materials, PMMA and aluminum, with 2 M methanol solution under 0.1 mL min^{-1} methanol flow rate, when the same heat amount is applied.

results, it can be observed that the PMMA, as the material of holders, is advantageous to maintaining the cell operating temperature and reducing the thermal loss, especially the thermal convection and radiation, due to its lower thermal conductivity coefficient.

5. Conclusions

A silicon-based μDMFC integrated with a temperature control system, consists of a heater and a temperature sensor is presented. A thermal model of the μDMFC is developed based on heat transfer and emission mechanisms in order to estimate the thermal behavior. The pattern of heater is optimally designed to improve the heating effect. The anode and cathode plates integrated with temperature control devices are fabricated using MEMS technologies. The μDMFC with optimized temperature control system is assembled by PDMS material and PMMA holders, and characterized in two methods, one with different currents applied and another with different methanol velocities. A μDMFC with a heater of different pattern and another assembled by aluminum holders, are tested to compare the heating effect and the temperature maintaining of packaging material. The heater of square pattern provides a more uniform temperature profile. The PMMA holders are used to not only protect the fragile silicon plates, but also reduce the thermal loss due to its lower thermal conductivity coefficient. This work would make it possible for a μDMFC to enhance the performance by adjusting to an optimal temperature and employ in extreme environments.

Acknowledgements

The authors would like to thank the National Natural Science Foundation of China (no. 90607014), National Basic Research Program of China (973 program, no. 2009CB320304), and the State Key Laboratory of Transducer Technology, Chinese Academy of Sciences.

References

[1] E. Sakaue, Tech. Digest MEMS Conference, Miami, USA, January 30–February 3, 2005, pp. 600–605.
[2] R. O'Hayre, S.-W. Cha, W. Colella, F.B. Prinz, Fuel Cell Fundamentals, first ed., John Wiley & Sons, New York, 2006, pp. 3–6.
[3] Gilbert Erdler, Mirko Frank, Mirko Lehmann, Holger Reinecke, Claas Muller, Sensors and Actuators A 132 (2006) 331–336.
[4] Y. Zhang, J. Lu, et al., Journal of Micromechanics and Microengineering 19 (2009) 015003.
[5] L.Y. Zhong, X.H. Wang, Y.Q. Jiang, Q. Zhang, Y.A. Zhou, X.P. Qiu, L.T. Liu, Sensors and Actuators A: Physical 143 (May (1)) (2008) 70–76.
[6] S.K. Kamarudin, W.R.W. Daud, S.L. Ho, U.A. Hasran, Journal of Power Sources 163 (2007) 743–754.
[7] Nam-Trung Nguyen, Siew Hwa Chan, Journal of Micromechanics and Microengineering 16 (2006) R1–R12.
[8] Hai Sun, Gongquan Sun, Suli Wang, Jianguo Liu, Xinsheng Zhao, Guoxiong Wang, Hengyong Xu, Shoufu Hou, Qin Xin, Journal of Membrane Science 259 (2005) 27–33.
[9] Yun-Ju Chuang, Ching-Chang Chieng, Chin Pan, Shih-Jin Luo, Fan-Gang Tseng, Journal of Micromechanics and Microengineering 17 (2007) 915–922.
[10] H. Dohle, J. Mergel, D. Stolten, Journal of Power Sources 111 (2002) 268–282.
[11] G.Q. Lu, C.Y. Wang, T.J. Yen, X. Zhang, Electrochim. Acta 49 (2004) 821–828.
[12] EunAe Cho, Jae-Joon Ko, Heung Yong Ha, Seong-Ahn Hong, Kwan-Young Lee, Tae-Won Lim, In-Hwan Oh, Journal of The Electrochemical Society 150 (12) (2003) A1667–A1670.
[13] Vladimir Neburchilov, Jonathan Martin, Haijiang Wang, Jiujun Zhang, Journal of Power Sources 169 (2007) 221–238.
[14] V.B. Oliveira, D.S. Falcão, C.M. Rangel, A.M.F.R. Pinto, International Journal of Hydrogen Energy 33 (2008) 3818–3828.
[15] Suhao He, Matthew M. Mench, Srinivas Tadigadapa, Sensor and Actuators A 125 (2006) 170–177.
[16] Chi-Yuan Lee, Shuo-Jen Lee, Ren-De Huang, Chih-Wei Chuang, Proceeding of the 7th IEEE International Conference on Nanotechnology, August 2–5, 2007, Hong Kong, 2007, pp. 1252–1255.
[17] M.M. Li, C. Liu, J.S. Liang, C.B. Wu, Z. Xu, Journal of Physics: Conference Series 48 (2006) 1078–1084.
[18] Q. Zhang, X.H. Wang, Y.A. Zhou, X.P. Qiu, L.T. Liu, Tech. Digest MEMS Conference, Sorrento, Italy, January 25–29, 2009, pp. 1107–1110.
[19] L. Zhong, X. Wang, Y. Jiang, et al., Sensors and Actuators A 143 (2008) 70–76.
[20] Yingqi Jiang, Xiaohong Wang, Lingyan Zhong, et al., Journal of Micromechanics and Microengineering 16 (2006) 233–239.
[21] Q. Zhang, X.H. Wang, L.Y. Zhong, Y.A. Zhou, X.P. Qiu, L.T. Liu, Tech. Digest MEMS Conference, Tucson, USA, January 13–17, 2008, pp. 972–975.